ChemComm

COMMUNICATION

View Article Online
View Journal | View Issue



Cite this: *Chem. Commun.*, 2023, 59, 11959

Received 4th August 2023,
Accepted 12th September 2023

DOI: 10.1039/d3cc03777k

rsc.li/chemcomm



# Simultaneously recorded photochemical action plots reveal orthogonal reactivity†

Ishrath Mohamed Irshadeen,[ab] Vinh X. Truong,[c] Hendrik Frisch *[ab] and Christopher Barner-Kowollik *[abd]

**We map the photochemical reactivity of two chromophores—a pyrene-chalcone and a methylene blue protected amine—from a one-pot reaction mixture based on their dynamic absorptivity changes upon light exposure, constructing a dual action plot. We employ the action plot data to determine a pathlength-independent λ-orthogonality window, allowing the orthogonal folding of distinct polymer chains into single chain nano-particles (SCNPs) from the same reaction mixture.**

Understanding photochemical reactivity as a function of the activation wavelength is critical for the design of precision photochemical reaction systems that respond to distinct colours of light in either a wavelength orthogonal, synergistic or antagonistic fashion.[1–3] Such highly selective photochemical systems hold significant potential for advanced applications such as light-activated 3D printing inks or curing processes, where disparate material properties can be generated from one photoresist entirely based on varying the colours of light.[4–7] Within the last decade, our team has developed a technology to map the wavelength-by-wavelength resolved photochemistry of covalent bond forming and cleaving reactions—known as photochemical action plots—demonstrating their utility in the design of advanced photoresponsive soft matter materials.[1] Perhaps the most pivotal finding that photochemical action plots have revealed is that the absorption spectrum of a chromophore is typically not an accurate predictor of its photochemical reactivity. In most cases, a red-shift in the photochemical reactivity is observed. The underpinning reasons for the mismatch between absorptivity and reactivity are currently explored, yet they are based on the fact that the absorption spectrum of a chromophore typically contains no information on excited state dynamics, in particular triplet states.[8] Indeed, other research teams have confirmed the strong red-shift of photochemical reactivity, including photo-induced reversible deactivation radical polymerization (RDRP).[9,10] The most notable example is a recent report from the group of Haddleton, showing quantitative conversions of $CuBr_2$/$Me_6$TREN mediated photopolymerization of methyl acrylates in spectral regions of near zero absorptivity.[10]

In addition to unravelling the wavelength resolved reactivity of photochemical reactions, we have applied photochemical reactions to construct complex macromolecules, including single chain nanoparticles (SCNPs),[11–14] which represent a contemporary research field.[15–17] SCNPs have been applied in catalysis[18–23] and sensors.[24,25] Light-driven reactions have been employed to construct and deconstruct SCNPs in a controlled fashion,[26–31] yet orthogonal folding of polymer chains into SCNPs using two distinct colours of light in a one-pot reaction system has not been achieved.

Herein, we utilise *trans*-pyrene-chalcone[32] and a methylene blue caged amine,[33] with well resolved absorbances, and simultaneously track their photoreactivity in a one-pot system to establish two orthogonality windows, wherein each of the moieties can be triggered to react independently irrespective of the sequence in which they are initiated. This strategy is motivated by three main considerations: (*i*) Using a mixture of the two desired chromophores allows to account for any effect of the changed light attenuation of the solution caused by the presence of another chromophore; (*ii*) chromophores may behave differently when in the same solution, *e.g.* by photosensitization; (*iii*) since every wavelength must be recorded and analysed separately, the recording of action plots is time-consuming, thus the simultaneous analysis of two species is more efficient.

[a] *School of Chemistry and Physics, Queensland University of Technology Faculty of Science and Engineering, Brisbane, Australia.*
*E-mail: christopher.barnerkowollik@qut.edu.au, h.frisch@qut.edu.au*
[b] *Centre for Materials Science, Queensland University of Technology (QUT), Brisbane, QLD 4000, Australia*
[c] *Institute of Sustainability for Chemicals, Energy and Environment (ISCE2), Agency for Science, Technology and Research (A*STAR), 1 Pesek Road, Jurong Island, Singapore 627833, Republic of Singapore*
[d] *Institute of Nanotechnology (INT), Karlsruhe Institute of Technology (KIT), Hermann-von-Helmholtz-Platz 1, Eggenstein-Leopoldshafen 76344, Germany*

† Electronic supplementary information (ESI) available: Synthetic procedures, action plot analysis details, molecular weight distributions. See DOI: https://doi.org/10.1039/d3cc03777k

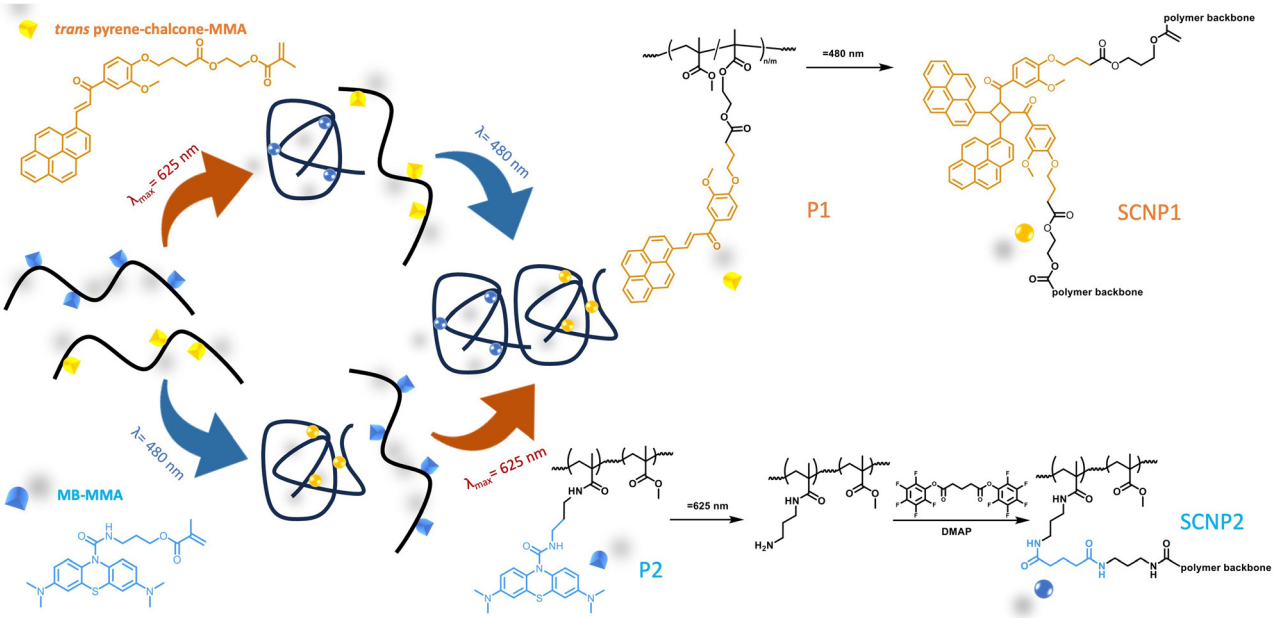


Scheme 1 Graphical depiction of the λ-orthogonal folding of two separate polymers (**P1** and **P2**) equipped with **MB-MMA** (blue) and **trans-pyrene-chalcone-MMA** (yellow), while in the same solution. **trans-pyrene-chalcone** undergoes [2+2] photocycloaddition at 480 nm within **P1**, while **MB** in **P2** stays photochemically silent, and is exclusively activated at 625 nm, leading to the uncaging of the amine group, which forms an amide bond with the crosslinker.

To translate the knowledge of the two orthogonality windows into SCNP folding, we incorporated the photoreactive monomers into separate polymers, which are capable of compacting *via* light-induced intramolecular crosslinking. In our design, one monomer unit carries a *trans*-pyrene-chalcone moiety able to undergo a [2+2] photocycloaddition,[32,34] while the other monomer unit carries a methylene blue photoprotected amine[33,35] (Scheme 1). The specific absorptivity profiles of these two monomer units—from which subsequently two distinct polymer chains are constructed for folding into SCNPs—is selected such that they do not overlap and, importantly, show a distinct change in their absorption spectrum upon irradiation, allowing their photochemical response to be tracked. Specifically, the *trans*-pyrene-chalcone containing monomer has only residual absorption above 450 nm, which decreases as the *trans*-pyrene-chalcone is consumed, while the methylene blue containing monomer only commences to absorb significantly post 525 nm, and the absorbance increases upon photocleavage of the caged amine, thus offering a unique opportunity to follow their photochemistry simultaneously.

Both chromophores are dissolved in equimolar quantities, which have a suitable absorbance for direct UV-vis measurements without further dilution and irradiated with an identical number of photons at pre-selected monochromatic wavelengths, in a procedure described in literature.[1] This analysis allows for the determination of the photochemical reactivity of both chromophores in a wavelength-resolved fashion, which is represented in a dual chromophore action plot. From this action plot, a λ-orthogonal photochemical reactivity window can be determined, where both chromophores can be independently activated to effect wavelength-orthogonal SCNP formation from a one-pot mixture containing both polymer chains carrying the respective chromophores (Scheme 1). Consequently, we selectively control the folding of polymer chains by two different wavelengths in a one-pot reaction mixture. We submit that the herein presented dual action plot technique allows for the facile reactivity mapping of specific photochemical reactions from one-pot reaction mixtures.

Fig. 1 depicts the dual action plot resulting from monitoring the individual change in absorptivity in the respective UV/Vis spectra of both chromophores (λ = 450 nm for **trans-pyrene-**

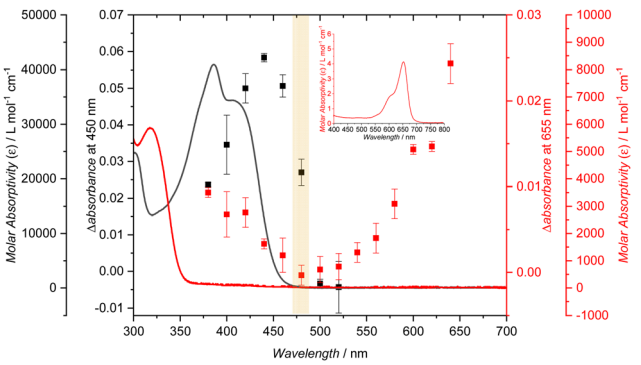


Fig. 1 Dual colour action plot for **MB-MMA** and **trans-pyrene-chalcone-MMA** as well as their absorption spectra. The red line line and inset depict $\varepsilon_{MB\text{-}MMA}$ whereas the black line depicts $\varepsilon_{Chalcone\text{-}MMA}$. The black squares represent the *Δabsorbance* at 450 nm representative of the depletion of *trans* pyrene-chalcone-MMA, while the red squares represent *Δabsorbance* at 655 nm representative of the photocleavage of MB-MMA. For each indicated wavelength 7.7 μmol of photons were deposited into the one-pot reaction system ($c_{MB\text{-}MMA}$ = 5.5 × $10^{-11}$ mol $L^{-1}$, $c_{Chalcone\text{-}MMA}$ = 5.5 × $10^{-11}$ mol $L^{-1}$ in acetonitrile).

 

**chalcone-MMA** and $\lambda$ = 655 nm for **MB-MMA**) in the same reaction mixture (refer to Fig. S17 and S18 for the time-resolved evolution of the absorption spectra for selected wavelengths as well as details of the spectral evaluation procedure to determine the relative change in absorptivity, ESI†). As the absorptivity of the amine-caged methylene blue unit is relatively weak, Fig. 1 also shows an enlargement of the relevant spectra region in the inset. The key findings from the action plots are: (*i*) The methylene blue chromophore displays a minimum of photochemical cleavage at close to 480 nm and effectively cleaves at longer, low energy wavelengths (650 nm); (*ii*) the reactivity of *trans*-pyrene-chalcone displays a significant red-shift,[32] allowing to identify a wavelength, *i.e.* 480 nm, at which *trans*-pyrene-chalcone reacts and the methylene blue shows almost no photocleavage (indicated by the highlighted area in Fig. 1). Thus, it is possible to identify two wavelengths, which allow addressing both chromophores fully pathway independently, *i.e.* 480 nm (predominant activation of the *trans*-pyrene-chalcone moiety) and 650 nm (exclusive activation of the methylene blue entity). To corroborate these findings, we recorded the conversion of each chromophore in the same reaction mixture at higher concentrations at the critical wavelength of 480 nm *via* $^1$H NMR spectroscopy and found that the *trans*-pyrene-chalcone was depleted by 47%, while the methylene blue unit was only converted by approximately 2%, thus supporting the UV/Vis absorption spectra driven analysis (refer to the ESI,† Section S4.3 and Fig. S21 for the $^1$H-NMR spectra and their associated conversion determination). To assess the kinetics of the orthogonal photocleavage, a solution of **MB-MMA** (0.27 mg mL$^{-1}$, 0.59 mmol L$^{-1}$) was irradiated with monochromatic light at 480 nm for, followed by monochromatic light at 640 nm, keeping the total number of photons delivered identical at both wavelengths ($1.98 \times 10^{19}$ photons) and the progress of the photocleavage was tracked *via* UV-Vis spectroscopy (ESI,† Section S4.2 and Fig. S19). The absorbance at 655 nm only increased from 0.016 to 0.019 over 30 min of irradiation at 480 nm, whereas the absorbance increased steeply from 0.019 to 0.052 upon switching the irradiation wavelength to 640 nm over the same time duration, critically supporting the orthogonality window at 480 nm. It is important to note that identifying a wavelength where the higher energy gated chromophore does not activate the lower energy species is rare, with the only three examples reported by our team.[5,36,37]

Subsequently, we copolymerised **MB-MMA** or **trans-pyrene-chalcone-MMA** with methyl methacrylate, to generate two polymers that can undergo light-induced folding into SCNPs at orthogonal wavelengths as determined in the above dual action plot analysis. The *trans*-pyrene-chalcone and MB containing polymers (**P1** and **P2**, respectively, refer to the ESI,† Sections S2.4 and S2.5) were jointly dissolved in acetonitrile and initially irradiated within the window of orthogonal reactivity ($\lambda$ = 480 nm), to investigate their orthogonal folding into SCNPs. The SEC refractive index (RI) trace of the mixture shows a maximum at 23.2 min elution time, which aligns with the elution time of **P2** (Fig. 2A, inset), and a shoulder at 24.2 min aligning with the elution time of **P1** (23.9 min, Fig. 2A, inset).

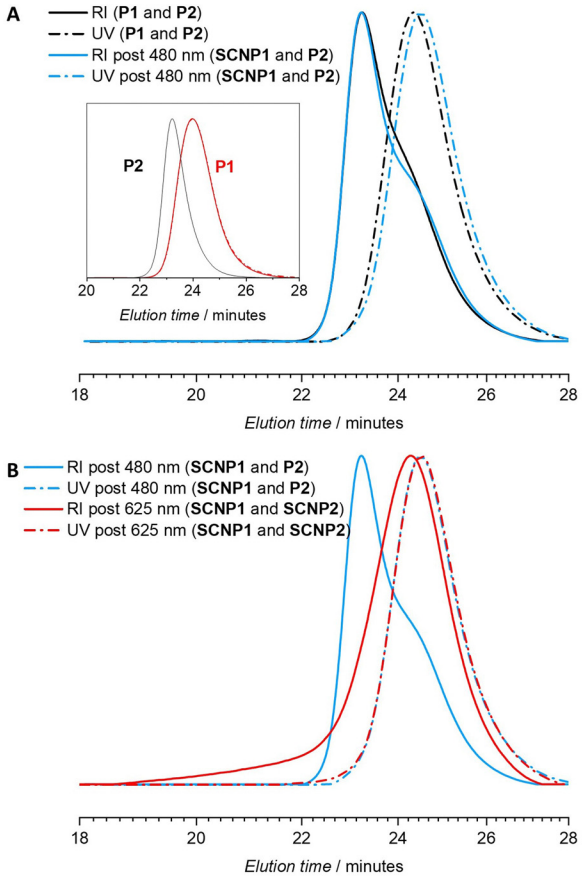


Fig. 2 (A) RI size-exclusion chromatograms (SEC) and UV trace (detection set to $\lambda$ = 360 nm) of **P1**, **P2** and **SCNP1** before and after irradiation at $\lambda$ = 480 nm (inset: separate elution times of **P1** and **P2**). (B) RI SEC and UV trace (UV detection set to $\lambda$ = 360 nm) of **SCNP1** and **SCNP2** after irradiation at $\lambda_{max}$ = 625 nm following initial irradiation at $\lambda$ = 480 nm.

Importantly, the UV-vis detector trace recorded at 360 nm is highly sensitive to **P1** due to its significantly higher molar extinction coefficient ($2.5 \times 10^4$ L mol$^{-1}$ cm$^{-1}$ for **trans-pyrene-chalcone-MMA** compared to 34 L mol$^{-1}$ cm$^{-1}$ for **MB-MMA** at $\lambda$ = 360 nm), which can be used to monitor the changes in the elution time of **P1**. Upon irradiation at 480 nm, the UV-vis detector trace of the SEC showed a significant shift towards later elution times, indicating the folding of **P1** into **SCNP1** upon intramolecular [2+2] photocycloaddition, substantiated by the appearance of pyrene peaks of the photocycloadducts at 331 and 350 nm in the UV-vis spectrum after 15 min of irradiation at 480 nm (Fig. S22, ESI†).[32]

The elution maximum of the RI trace assigned to **P1**, however, did not shift towards longer elution times, only the shoulder at later elution times assigned to **P2** shifted. After subsequent irradiation at 640 nm, the RI trace maximum shifted by more than 1 min to 24.2 min, indicating the folding of **P2** into **SCNP2**, while the UV-vis trace did not shift any further. These results indicate the orthogonal and complete folding of **P1** at the high energy wavelength without affecting **P2**. Orthogonal folding in the reverse order of irradiation, *i.e.* low to high energy, was subsequently investigated using an

identical mixture of **P1** and **P2** (ESI,† Section S3.2). Irradiation at 640 nm led to the previously observed shift in RI trace of $>$ 1 min, whereas the UV-vis trace remained unchanged, indicating the selective folding of **P2**. Subsequent irradiation at 480 nm, yields no observable shift of the RI trace, however, displays the previously observed shift of the UV trace indicating the folding of **P1** into **SCNP1**. The folding of **P1** and **P2** can thus be independently induced within the determined orthogonality windows as a function of wavelength and, importantly, in any order. Notably, photocycloaddition reactions are strongly concentration dependent. At the low concentrations of the dual-action plot measurement, photoisomerization likely dominates the observed depletion rather than photocycloaddition.[27,38] However, the recorded action plot shows the same reactivity maximum as for the photocycloaddition and allows to determine the orthogonality window for the selective photocycloaddition within **P1**,[32] illustrating that the depletion serves as an effective proxy for photocycloaddition.

In conclusion, we introduce a technique to simultaneously map the wavelength-resolved photochemical reactivity of two chromophores jointly present in the same reaction mixture by following the change in their non-overlapping absorption spectra, yielding a dual-photochemical action plot. The outcome is critical for identifying a wavelength at which the more red-shifted photochemical reactant remains photochemically silent, while the blue-shifted reactant is activated, thus allowing for orthogonal wavelength reactivity. We exemplify the power of our dual photochemical action plot technique by pathway independently folding two polymer chains carrying one of each chromophore into single chain nanoparticles (SCNPs) from a one-pot reaction mixture.

C. B.-K. and H. F acknowledge funding from the Australian Research Council (ARC) in the form of a Laureate (C. B.-K. FL170100014) and DECRA Fellowship (H. F) as well as continued key support from the Queensland University of Technology (QUT). I. M. I. acknowledges QUT for a PhD scholarship.

## Conflicts of interest

There are no conflicts to declare.

## Notes and references

1 I. M. Irshadeen, S. L. Walden, M. Wegener, V. X. Truong, H. Frisch, J. P. Blinco and C. Barner-Kowollik, *J. Am. Chem. Soc.*, 2021, **143**, 21113–21126.
2 J. Hobich, E. Blasco, M. Wegener, H. Mutlu and C. Barner-Kowollik, *Macromol. Chem. Phys.*, 2023, **224**, 2200318.
3 N. Corrigan, M. Ciftci, K. Jung and C. Boyer, *Angew. Chem., Int. Ed.*, 2021, **60**, 1748–1781.
4 N. D. Dolinski, Z. A. Page, E. B. Callaway, F. Eisenreich, R. V. Garcia, R. Chavez, D. P. Bothman, S. Hecht, F. W. Zok and C. J. Hawker, *Adv. Mater.*, 2018, **30**, 1800364.
5 S. Bialas, L. Michalek, D. E. Marschner, T. Krappitz, M. Wegener, J. Blinco, E. Blasco, H. Frisch and C. Barner-Kowollik, *Adv. Mater.*, 2019, **31**, 1807288.
6 P. Lu, D. Ahn, R. Yunis, L. Delafresnaye, N. Corrigan, C. Boyer, C. Barner-Kowollik and Z. A. Page, *Matter*, 2021, **4**, 2172–2229.
7 Z. Zhang, N. Corrigan and C. Boyer, *Angew. Chem., Int. Ed.*, 2022, **61**, e202114111.
8 J. P. Menzel, B. B. Noble, A. Lauer, M. L. Coote, J. P. Blinco and C. Barner-Kowollik, *J. Am. Chem. Soc.*, 2017, **139**, 15812–15820.
9 J. A. Reeves, N. De Alwis Watuthanthrige, C. Boyer and D. Konkolewicz, *ChemPhotoChem*, 2019, **3**, 1171–1179.
10 C. Ma, T. Han, S. Efstathiou, A. Marathianos, H. A. Houck and D. M. Haddleton, *Macromolecules*, 2022, **55**, 9908–9917.
11 H. Frisch, B. T. Tuten and C. Barner-Kowollik, *Isr. J. Chem.*, 2020, **60**, 86–99.
12 W. Kuhn and G. Balmer, *J. Polym. Sci.*, 1962, **57**, 311–319.
13 E. Harth, B. V. Horn, V. Y. Lee, D. S. Germack, C. P. Gonzales, R. D. Miller and C. J. Hawker, *J. Am. Chem. Soc.*, 2002, **124**, 8653–8660.
14 E. J. Foster, E. B. Berda and E. W. Meijer, *J. Am. Chem. Soc.*, 2009, **131**, 6964–6966.
15 A. P. P. Kröger and J. M. J. Paulusse, *J. Controlled Release*, 2018, **286**, 326–347.
16 R. Chen and E. B. Berda, *ACS Macro Lett.*, 2020, **9**, 1836–1843.
17 M. A. M. Alqarni, C. Waldron, G. Yilmaz and C. R. Becer, *Macromol. Rapid Commun.*, 2021, **42**, 2100035.
18 J. Chen, K. Li, S. E. Bonson and S. C. Zimmerman, *J. Am. Chem. Soc.*, 2020, **142**, 13966–13973.
19 J. Chen, J. Wang, K. Li, Y. Wang, M. Gruebele, A. L. Ferguson and S. C. Zimmerman, *J. Am. Chem. Soc.*, 2019, **141**, 9693–9700.
20 A. Sathyan, S. Croke, A. M. Pérez-López, B. F. M. de Waal, A. Unciti-Broceta and A. R. A. Palmans, *Mol. Syst. Des. Eng.*, 2022, **7**, 1736–1748.
21 H. Rothfuss, N. D. Knöfel, P. W. Roesky and C. Barner-Kowollik, *J. Am. Chem. Soc.*, 2018, **140**, 5875–5881.
22 J. Rubio-Cervilla, E. González and J. A. Pomposo, *Nanomaterials*, 2017, **7**, 341.
23 K. Mundsinger, B. T. Tuten, L. Wang, K. Neubauer, C. Kropf, M. L. O'Mara and C. Barner-Kowollik, *Angew. Chem., Int. Ed.*, 2023, **62**, e202302995.
24 L. Deng, L. Albertazzi and A. R. A. Palmans, *Biomacromolecules*, 2022, **23**, 326–338.
25 A. B. Benito, M. K. Aiertza, M. Marradi, L. Gil-Iceta, T. Shekhter Zahavi, B. Szczupak, M. Jiménez-González, T. Reese, E. Scanziani, L. Passoni, M. Matteoli, M. De Maglie, A. Orenstein, M. Oron-Herman, G. Kostenich, L. Buzhansky, E. Gazit, H.-J. Grande, V. Gómez-Vallejo, J. Llop and I. Loinaz, *Biomacromolecules*, 2016, **17**, 3213–3221.
26 D. Kodura, L. L. Rodrigues, S. L. Walden, A. S. Goldmann, H. Frisch and C. Barner-Kowollik, *J. Am. Chem. Soc.*, 2022, **144**, 6343–6348.
27 H. Frisch, J. P. Menzel, F. R. Bloesser, D. E. Marschner, K. Mundsinger and C. Barner-Kowollik, *J. Am. Chem. Soc.*, 2018, **140**, 9551–9557.
28 D. Kodura, H. A. Houck, F. R. Bloesser, A. S. Goldmann, F. E. Du Prez, H. Frisch and C. Barner-Kowollik, *Chem. Sci.*, 2021, **12**, 1302–1310.
29 O. Galant, H. B. Donmez, C. Barner-Kowollik and C. E. Diesendruck, *Angew. Chem., Int. Ed.*, 2021, **60**, 2042–2046.
30 H. Frisch, D. Kodura, F. R. Bloesser, L. Michalek and C. Barner-Kowollik, *Macromol. Rapid Commun.*, 2020, **41**, 1900414.
31 W. Fan, X. Tong, Q. Yan, S. Fu and Y. Zhao, *Chem. Commun.*, 2014, **50**, 13492–13494.
32 I. M. Irshadeen, K. De Bruycker, A. S. Micallef, S. L. Walden, H. Frisch and C. Barner-Kowollik, *Polym. Chem.*, 2021, **12**, 4903–4909.
33 I. Mohamed Irshadeen, V. X. Truong, H. Frisch and C. Barner-Kowollik, *Chem. Commun.*, 2022, **58**, 12975–12978.
34 M. Van De Walle, K. De Bruycker, J. P. Blinco and C. Barner-Kowollik, *Angew. Chem., Int. Ed.*, 2020, **59**, 14143–14147.
35 H. M. Dao, C.-H. Whang, V. K. Shankar, Y.-H. Wang, I. A. Khan, L. A. Walker, I. Husain, S. I. Khan, S. N. Murthy and S. Jo, *Chem. Commun.*, 2020, **56**, 1673–1676.
36 P. W. Kamm, L. L. Rodrigues, S. L. Walden, J. P. Blinco, A.-N. Unterreiner and C. Barner-Kowollik, *Chem. Sci.*, 2022, **13**, 531–535.
37 H. Frisch, F. R. Bloesser and C. Barner-Kowollik, *Angew. Chem., Int. Ed.*, 2019, **58**, 3604–3609.
38 B. J. Richardson, C. Zhang, P. Rauthe, A.-N. Unterreiner, D. V. Golberg, B. L. J. Poad and H. Frisch, *J. Am. Chem. Soc.*, 2023, **145**, 15981–15989.

 